THE ASTROPHYSICAL JOURNAL, 249:704–719, 1981 October 15

TIME ASYMMETRIES IN PULSAR SIGNALS

D. STINEBRING AND J. M. CORDES
National Astronomy and Ionosphere Center, and Department of Astronomy, Cornell University
Received 1980 November 21; accepted 1981 April 22

ABSTRACT

We present a technique for analyzing time asymmetries of stochastic processes and apply it to high time resolution data from pulsars PSR 0950+08 and PSR 2016+28. Subpulses and average waveforms show similar time asymmetries. This is consistent with subpulses arising from beams of radiation rather than temporal modulations. Micropulses are, on average, time symmetric. It is possible that individual micropulses are asymmetric, but over a data set of several hundred pulses, there is no preferred sense of asymmetry.

Subject heading: pulsars

I. INTRODUCTION

Pulsar observations of increasingly high time resolution have always held the promise of a direct look at the coherent radio emission mechanism. Unfortunately, it is becoming clear that pulsars hide the details of the emission process behind a cover of incoherent superposition, removing all traces of the underlying coherence except for the enormous brightness temperature. Investigations of the statistical properties of the pulsar intensity (Cordes 1976; Hankins and Boriakoff 1978; Cordes and Hankins 1979) show that the emission can be well modeled as amplitude modulation of a complex Gaussian noise process, the so-called amplitude modulated noise model (AMN) first presented by Rickett (1975). A major implication of the AMN model is that micropulse emission (typically submillisecond fluctuations in the amplitude envelope) may remain the shortest physically meaningful fluctuation of the radio emission—even though observations are now available (such as those of Hankins and Boriakoff 1978) with submicrosecond time resolution.

Given the above statistical character of micropulses it is important to investigate their physical basis. What sort of mechanism gives rise to these exceedingly brief and intense glimpses at the emission process? Models for micropulse emission can be divided into two broad classes—"temporal models" in which the intensity fluctuation is caused by an actual modulation of the radiation beam, and "beaming models" in which the pulsar's rotation sweeps a constant pencil beam across the line of sight. Unsteadiness in the current injection process near the surface of the neutron star would be an example of the first class. Indeed, fluctuations in the flow of primary ions and the rate of electron-positron pair creation have been proposed (Cheng and Ruderman 1980; Ruderman and Sutherland 1975). The rise and fall of plasma instabilities in the near magnetosphere, such as beam-plasma instabilities or the formation of solitons, are other examples of this class.

In the second class, beaming models, the micropulse emission is primarily a geometrical phenomenon. For example, Benford (1977) sees micropulse emission as the sweep of our line of sight across a series of radiating plasma filaments that are parallel to the field lines. Other models have different explanations for the beaming of radiation along the field lines (e.g., coherent curvature radiation), but concur in viewing a micropulse as just the angular sweep of this beam past the observer. It should be noted that Ferguson (1979) and Kirk and ter Haar (1978) also view the microstructure as essentially a beaming phenomenon, but one arising from relativistic beaming by bunches of particles near the light cylinder.

The two general classes of micropulse models may have different observational implications. Although an investigation of the full polarization behavior of micropulses, especially the variation of the polarized emission within micropulses, provides a fuller probe of these models, we restrict ourselves in this paper to the intensity envelope of these features. In particular, we present a technique for analyzing the temporal symmetry of micropulse envelopes, looking for any systematic deviation from perfectly symmetrical micropulses.

The physical motivation for this analysis grows from the qualitative difference between the two classes of micropulse models noted above. If the micropulses are primarily a temporal phenomenon, there is no *a priori* reason to expect the micropulse rise and decay time scales to be identical. For example, in the case of a plasma instability the rise time of the fluctuation is governed by the growth rate of the particular instability,

whereas the decay time scale involves the rate at which the accumulated energy can be transferred to electromagnetic wave modes.

Beaming models of micropulse emission, on the other hand, may more easily produce symmetric micropulse envelopes. Even if the local field geometry at the point of emission differs from a simple dipolar approximation—as it almost certainly does close to the star—the main effect is a tilting of the cone of emission rather than the introduction of time asymmetry into the micropulse profile.

The average shape of subpulses is also of interest. Since subpulse emission is, in general, composed of both a micropulse component and a more continuous, uniform emission, care is needed in interpreting subpulse shapes physically. A number of questions can be raised. For example, what is the relationship between subpulse and average waveform shape? It is not known whether asymmetry in subpulses contributes to asymmetry in the average waveform or whether asymmetric average waveforms are constructed from symmetric subpulses with an asymmetrical probability of occurrence in pulse longitude.

The analysis technique that we present here allows us to investigate the shape and time symmetry properties of both the micropulse and subpulse emission features. In § II of this paper we outline our analysis procedure and apply it to simulated pulsar data. In § III we analyze a series of pulses from PSR 0950+08 and PSR 2016+28, using dedispersed data with microsecond time resolution. Finally, in § IV we discuss the implications of our analysis for the physical processes underlying both micropulse and subpulse emission. The Appendix contains the mathematical details of our skewness analysis technique, concentrating on the intermingling of time scales in the analysis and on the calculation of estimation errors.

II. SKEWNESS ANALYSIS

a) Measures of Time Asymmetries

There are a number of possible ways to measure any time asymmetry in the micropulse and subpulse features. The most direct method would be to identify individual micropulse or subpulse features and parameterize their intensity profiles. This method suffers from two problems, however: the difficulty of isolating overlapping features and the difficulty of finding a bias-free model-fitting procedure for a profile whose general shape is not known *a priori*. Both difficulties become rapidly more severe as the signal-to-noise ratio of the data decreases.

Consequently, we are led to a method which does not rely on identifying individual time series features. In addition, because of the large amount of data involved and the expected stochastic nature of the emission process, we concentrate on statistical estimations of the emission skewness properties. In so doing we build on the existing second-order analyses of micropulses (Cordes 1976) and adopt a procedure similar to that used by Weisskopf *et al.* (1978) in studying the $1-s$ pulses from the X-ray source Cygnus X-1.

The mathematical details of this analysis are contained in the Appendix, but a simple description of the technique is in order here. The simplest second-order correlation is the autocorrelation function, which yields information about the time scales and periodicities of various features in the time series, but contains no information about the skewness of individual features since it is symmetric about the origin. The simplest third-order correlation, however, in which the square of the time series is correlated with the original function,

$$T_I(\tau)=\int dt\, I(t)I^2(t+\tau), \tag{1}$$

where $I(t)$ is the time series in question, is not in general symmetric about the origin. We show in the Appendix that this lack of symmetry about the origin can be interpreted directly in terms of the symmetry properties of the emission features. If $T_I^+(\tau)$ and $T_I^-(\tau)$ represent the positive and negative lag halves of the third-order correlation [i.e., $T_I^{\pm}(\tau)\equiv T_I(\pm\tau)$], then our definition of the skewness function is simply

$$K_I(\tau)\equiv T_I^+(\tau)-T_I^-(\tau), \tag{2}$$

which can be normalized by analogy with second-order correlations as

$$K_I(\tau)\equiv K_I(\tau)/T_I(0). \tag{3}$$

An excursion of this normalized skewness function away from zero results from asymmetrical emission features in the time series, the time scale of the excursion corresponding to that of the time series feature being probed. Positive (negative) values of the skewness function represent emission features whose rise times are smaller (larger) than their decay times. This procedure automatically combines skewness information from the various emission features within a given pulse, discarding the phase information from them. We are thus able to determine any systematic deviations from symmetry in both micropulses and subpulses without having to identify them individually.

b) Simulated Data

We tested the analysis technique by applying it to simulated pulsar data. We generated pulsar pseudopulses using the AMN model as an empirical description of the intensity fluctuations. As further discussed in the Appendix, this allows the separation of the pulsed

emission into multiplicative components which are then combined with a Gaussian noise generator to create the intensity time series. We use a simulation with only two basic components: a deterministic average waveform and a stochastic micropulse shot sequence.

For a particular realization of this random process (i.e., for a particular simulated pulse), the product of the average waveform and the micropulse shot train form the amplitude modulation. The micropulse shot sequence is the convolution of a Poisson-distributed series of impulse functions with a deterministic "shape function." This amplitude envelope is then used to modulate a complex Gaussian noise process, simulating an actual pulsar pulse that is sampled at the Nyquist rate (Rickett 1975). Gaussian noise can also be added to this signal so as to account for receiver and background sky noise with a specified signal-to-noise ratio.

Referring to Figure 1 we see the results of one such simulation with an asymmetrical average waveform. The micropulse shape function is also asymmetrical, being a triangle with the base of the leading portion twice as long as that of the trailing portion. The filling factor of the micropulse shot train, which is defined as

$$f \equiv \eta W_\mu, \tag{4}$$

where W_μ is the micropulse width and η is the micropulse occurrence rate, was chosen to be 0.25 for this simulation. Finally, the signal-to-noise ratio averaged over the pulse was set to be close to that characterizing the real pulsar data analyzed in § III.

The results of the skewness analysis are shown on the right-hand side of Figure 1. Three skewness curves are shown: one of the average waveform itself and two (high and low resolution) curves for simulated pulses. The skewness function of the waveform is negative because it rises more slowly than it decays. In the low resolution curve, both the micropulse and the average waveform asymmetries are identifiable because of the difference in their time scales. The high resolution curve shows the micropulse skewness in more detail.

In both the low resolution and high resolution curves, estimation errors are due primarily to the finite number of pseudo pulses (1200) rather than to the finite signal-to-noise ratio. This estimation error can be understood as the result of two effects. The first arises from overlapping features that affect the *shape* of the skewness function. In the simulation (with a relatively small filling factor) this effect is small. The second source of estimation error is due to exceptionally strong micropulses that cause the *amplitude* of the skewness function to be misestimated. Although the effect of any one contribution will eventually be balanced out in the averaging process (at least in this simulation where the AMN is strictly adhered to), it is not easy to estimate how many pulses need to be averaged in order to stabilize the skewness curves. This has proven to be one of the most useful features of the simulated data analysis: the simulation allows an empirical investigation of the estimation error.

Note that it is the first form of estimation error that has led us to adopt a statistical skewness averaging technique rather than investigating individual micropulses. Micropulse features are almost never completely isolated from overlapping subpulse, micropulse, or other "baseline" emission. The presence of *sloping* baseline emission will bias individual micropulse skewness functions, typically by an additive term (in the normalized skewness function) of order $\Delta b/h_\mu$, where Δb is the difference in baseline height across the micropulse of height h_μ. This confusion term can significantly and irretrievably alter the normalized skewness function for an individual micropulse because of the uncertainty in subtracting baseline emission from a micropulse feature. The statistical averaging technique that we employ is, however, much less vulnerable to local baseline emission, since the skewness function of independent random processes can be separated into independent skewness terms (see Appendix, particularly eq. [A34]).

It should be pointed out that *unsloped* baseline emission will also have an effect on the value of the normalized skewness function. Although such emission introduces no new skewness, it does alter the magnitude of the uncorrupted skewness function by biasing the normalizing denominator $T_I(0)$. A misestimation of the off-pulse signal mean could, for example, introduce such an effect. However, the autocorrelation function is even more sensitive to this sort of biasing, and, as we shall show in § III, there is no evidence (such as the autocorrelation not approaching zero for large lag values) that our results are significantly influenced by this effect.

III. APPLICATION TO TWO PULSARS

a) PSR 0950+08

This nearby pulsar is sporadic in its emission characteristics, radiating in bursts of about 10 pulses whose amplitude distribution has a long tail (Ritchings 1976; Hankins and Cordes 1981). We have analyzed 240 pulses obtained at 430 MHz (see Table 1). The data were software dedispersed (Hankins and Rickett 1975) so that no interstellar dispersion broadening is present. The effect of interstellar scattering as a broadening agent is not important in our analysis of this pulsar at 430 MHz. Armstrong and Rickett (1981) estimate the decorrelation bandwidth at this frequency to be >2 MHz which results in a scattering time scale of <0.1 μs.

The pulses were analyzed in blocks of 60 pulses. The variation in skewness profiles from block to block gives a good idea of the estimation error present in the analysis. The differences between blocks were negligible compared to the features common to all of the blocks.

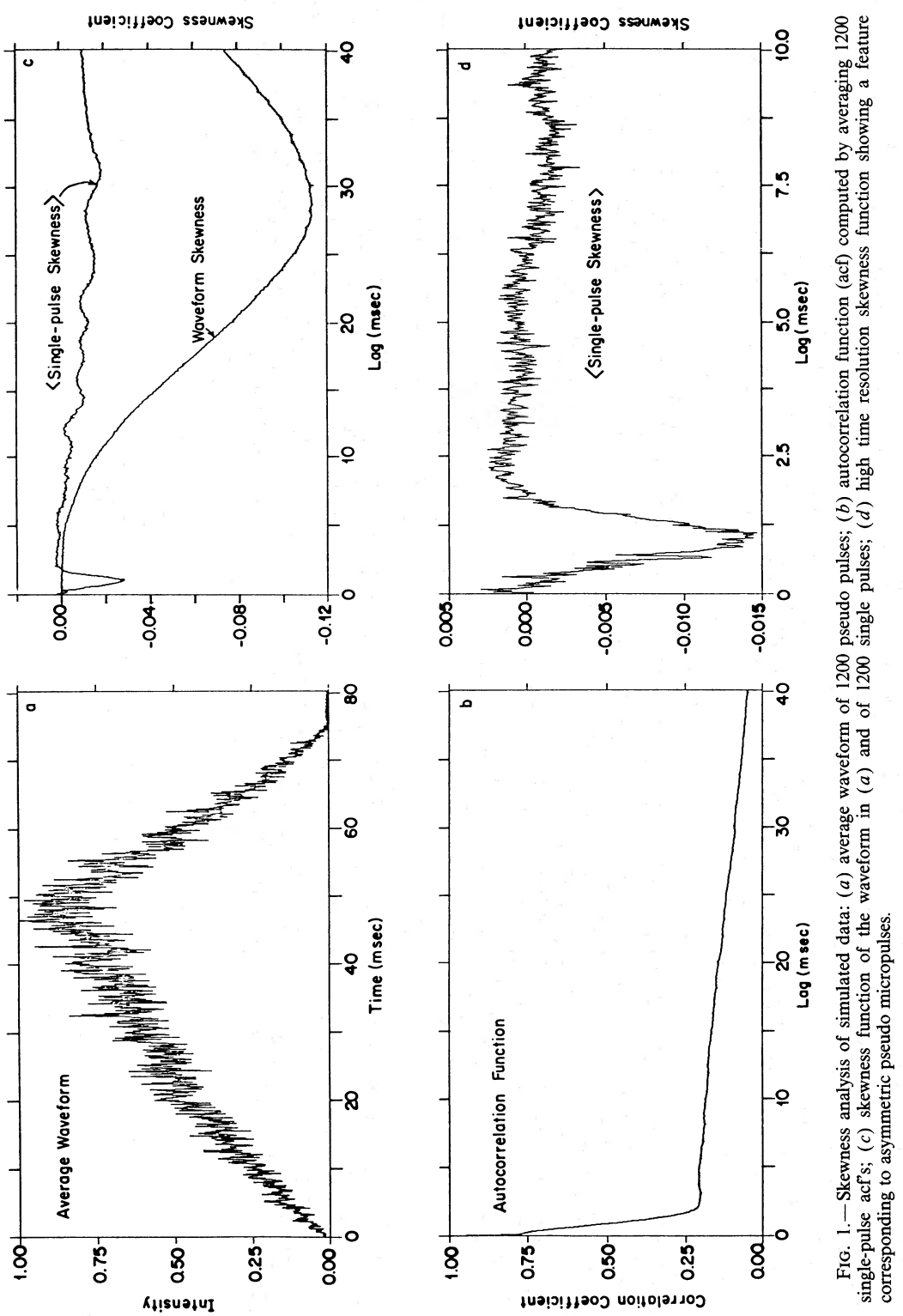

FIG. 1.—Skewness analysis of simulated data: (*a*) average waveform of 1200 pseudo pulses; (*b*) autocorrelation function (acf) computed by averaging 1200 single-pulse acf's; (*c*) skewness function of the waveform in (*a*) and of 1200 single pulses; (*d*) high time resolution skewness function showing a feature corresponding to asymmetric pseudo micropulses.

TABLE 1

OBSERVING PARAMETERS

Pulsar	Date	Number of Pulses	Time Resolution (μs)	Polarization
PSR 0950+08 ...	1976 May	240	0.8	LCP
PSR 2016+28 ...	1976 June	978	7.0	LCP

The average signal-to-noise ratio for these pulses, defined as

$$\mathrm{SNR} \equiv \frac{\langle I \rangle_{\mathrm{on}} - \langle I \rangle_{\mathrm{off}}}{\langle I \rangle_{\mathrm{off}}}, \qquad (5)$$

(where on and off refer to on-pulse and off-pulse averages) is ~ 2.2. This average value, though, does not account for the extremely localized character of the micropulse emission. The micropulses generally occur (with filling factors between 0.1 and 0.5) in subpulse groups which typically fill only 30% of the pulse window. Therefore, the signal-to-noise ratio of a micropulse peak is typically >20.

i) *Skewness of a Single Pulse*

The skewness properties of a single pulse are shown in Figure 2. The left-hand side of this figure shows a low and high resolution picture of the pulse. Notice the sharp discontinuity near the center of this pulse, a common feature in this pulsar, with the breaks occurring at random longitudes. The right-hand panels show the corresponding skewness functions for the low (subpulse) and high (micropulse) resolution data. For positive intensity data the range of the skewness function is ± 1.

Most of the 0.1 ms fluctuations in the low resolution skewness curve are estimation errors, but it is interesting to see the correspondence between the time series and the skewness curve. Of particular note is the bimodal structure (first a positive excursion followed by a stronger negative feature), due to the presence of two subpulses in this pulse. The initial positive feature is the sum of both the leading and trailing subpulse skewnesses. The skewness curve of the first subpulse alone would be negative because the emission rises more slowly than it decays. Conversely, the more sharply angled second feature would individually have a positive skewness. Since this second subpulse is stronger and more skewed, its contribution to the skewness function is greater; the pulse taken as a whole then has an initially positive skewness. For time lags slightly greater than the subpulse feature widths, the skewness curve returns momentarily to zero because the subpulses do not overlap. Once the correlation lag becomes large enough to start blending the two subpulse features we see a strong negative excursion.

The high resolution skewness curve displays a number of features, but it is clear in this pulse that the micropulse skewness function has a mean of zero. The intensity discontinuity in the pulse does not affect this curve significantly because it occurs over a time scale long compared to the range of time lags. Note, too, that the values of the skewness function are smaller for the high resolution curve than for the low resolution one. This is a consequence of our normalization (eq. [3]) by the zero-lag third moment which decreases as the data are smoothed.

ii) *Average Skewness*

The ensemble average data are summarized in Figure 3. The general features of the average waveform are clearly represented, with the steep falloff of emission in the second half of the pulse being a permanent feature of this pulsar's profile.

The skewness curve of the average waveform (the smoother curve in panel 3*c*) demonstrates quantitatively what the eye can distinguish in the profile qualitatively: the second half of the pulse falls off more rapidly than the pulse builds up (hence, the skewness function is negative).

The autocorrelation function, shown below the average profile, has the following features: a small zero-lag spike component which has been reduced in height from its critically sampled value of 0.5 by the averaging of the data over 32 samples (64 degrees of freedom). More significant is the "breakpoint" in the slope of the curve at ~ 120 μs lag, which is a characteristic value of the distribution of micropulse widths.

The heart of the analysis for PSR 0950+08 is shown in the average low and high resolution skewness functions. The low resolution curve still shows fluctuations on a 100–200 μs time scale, but these are due to estimation error. What is stable and significant is the negative excursion to a skewness value of -0.05 followed by an almost total return to the zero skewness level. This excursion indicates a systematic skewness of the subpulse features, with the rise time longer than the decay time. Notice that the subpulse skewness feature is both narrower and less pronounced than that of the average profile in Figure 3, indicating that a typical subpulse for PSR 0950+08 is both narrower in width and slightly more symmetrical than the average profile.

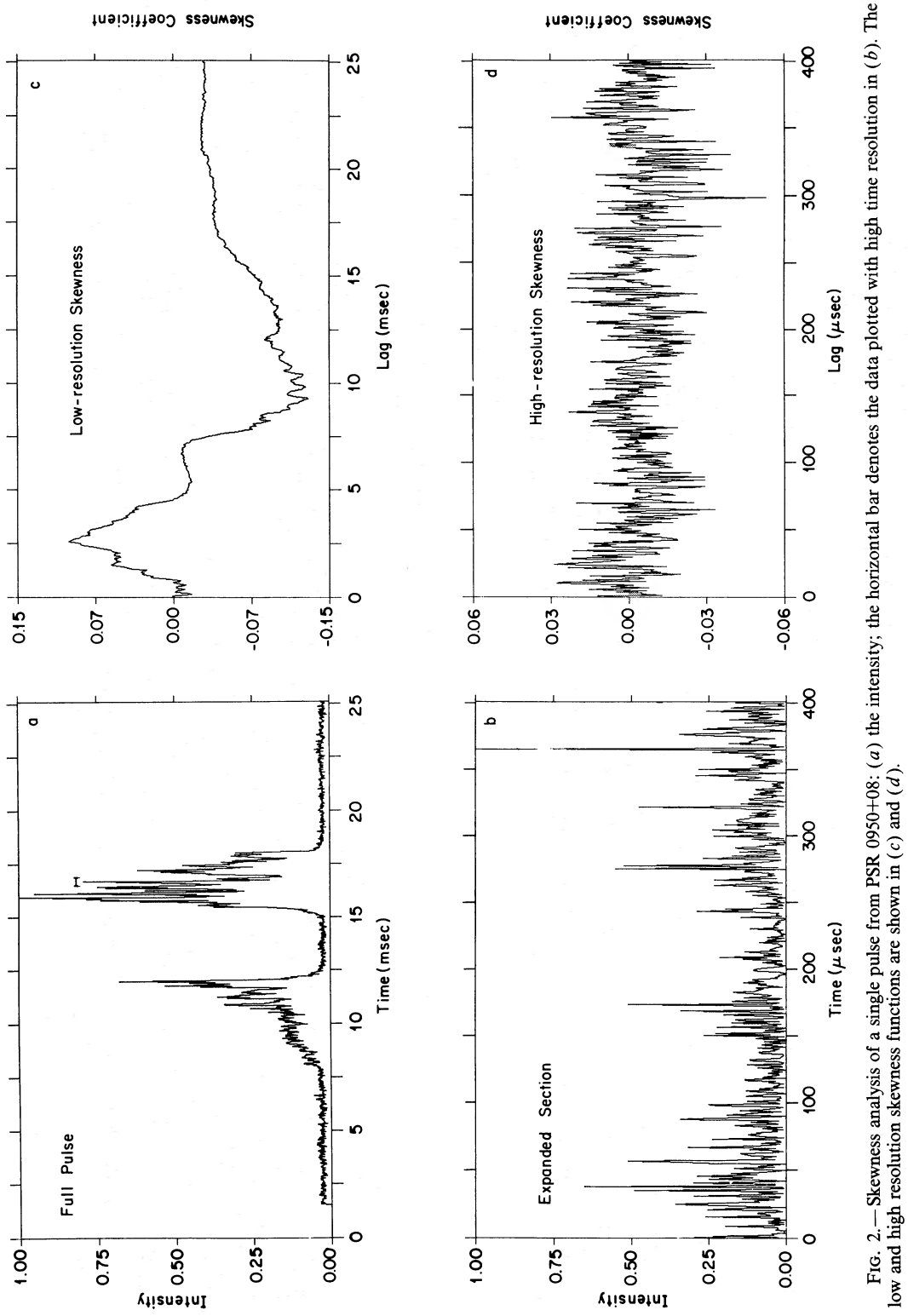

FIG. 2.—Skewness analysis of a single pulse from PSR 0950+08: (*a*) the intensity; the horizontal bar denotes the data plotted with high time resolution in (*b*). The low and high resolution skewness functions are shown in (*c*) and (*d*).

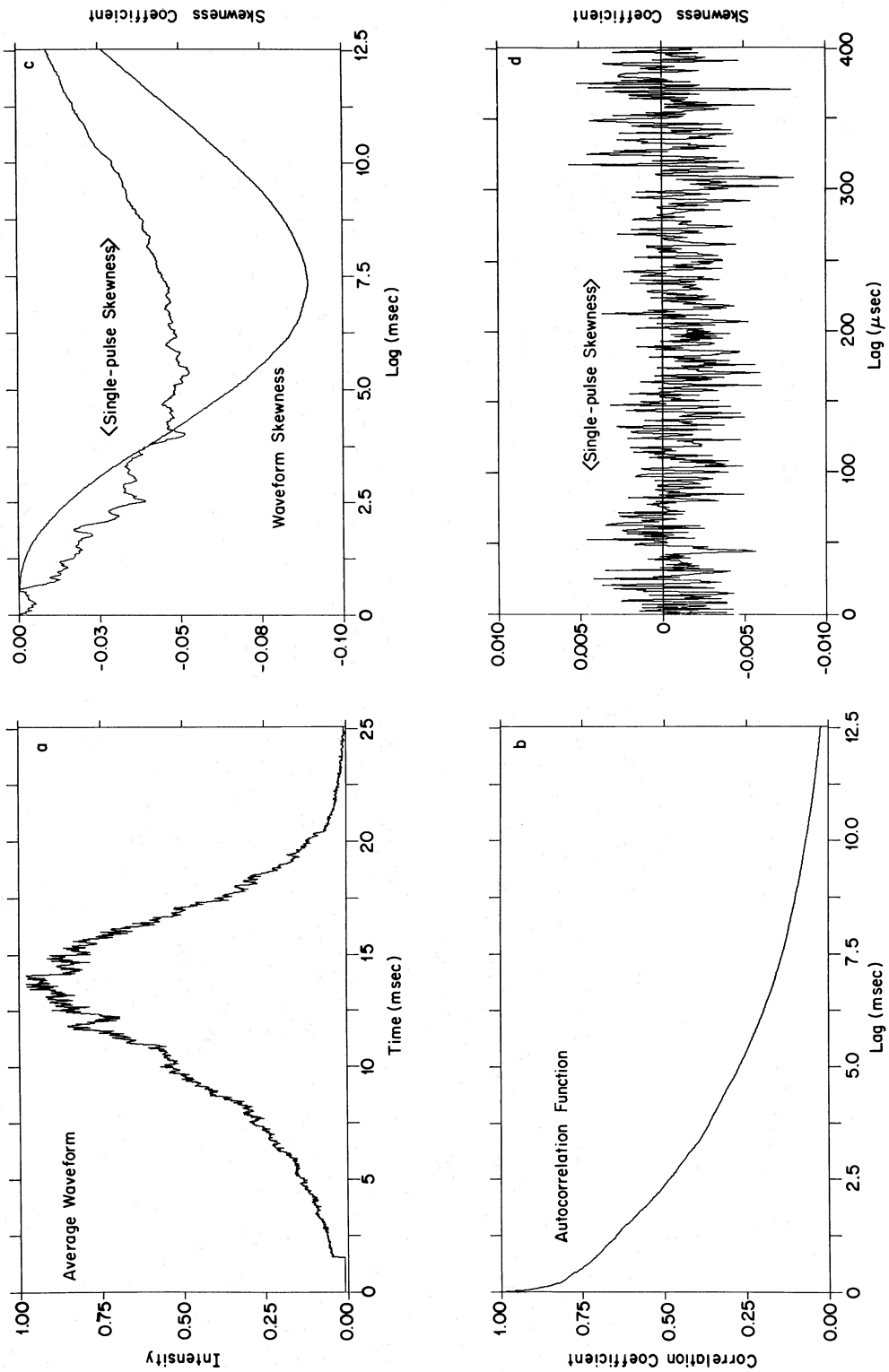

FIG. 3.—Average skewness analysis of 240 pulses from PSR 0950+08. The same quantities are plotted as in Fig. 1.

The high resolution skewness function displays a much simpler functional behavior. To a very high degree of sensitivity there seems to be no *systematic* skewness on micropulse time scales in the pulses we have analyzed. Note the sharp improvement in the estimation error here, since we are now dealing with micropulse contributions which significantly outnumber the subpulse contributions in a typical pulse. If the micropulse shape were even 10% as asymmetrical on the average as the total profile we would see a deflection in this skewness curve.

b) PSR 2016+28

Whereas PSR 0950+08 is sporadic in its emission, PSR 2016+28 produces a very narrow average pulse amplitude distribution, with no evidence of nulls (Ritchings 1976). It does, however, exhibit drifting subpulses. Taylor, Manchester, and Huguenin (1975) have shown that the subpulse drift bands change their slope in a manner that maintains a roughly constant separation ($P_2 \sim 10$ ms or 7° of longitude). This is in contrast to PSR 0950+08 which only occasionally has multiple subpulses within the window at a given time, and then with no particular phase relationship between the two.

The data for PSR 2016+28 have had the effect of dispersion smearing removed (yielding 7 μs time resolution) and are also not significantly affected by scattering in the interstellar medium because the 430 MHz decorrelation bandwidth of 70 KHz (Rickett 1977) implies a scattering time of ≈ 2 μs.

We analyzed a total of 978 pulses for PSR 2016+28, split into two blocks. Again, we saw no significant differences in these two blocks. The estimation error is smaller for this pulsar than for PSR 0950+08, both because of the greater number of pulses and because the emission is steadier.

Turning to the single pulse curves shown in Figure 4, we see a more complicated behavior than for PSR 0950+08. The low resolution intensity curve of the pulse chosen here shows the characteristic double subpulse structure mentioned above, with the two subpulses separated by ~ 11 ms. Likewise, in the low resolution skewness curve we see a double-troughed feature. As in Figure 2, the first trough represents the skewness of the individual subpulse features; the second feature is a "cross-skewness" of the two subpulses.

The high resolution skewness curve looks remarkably similar to that for PSR 0950+08 except that the estimation error is smaller. Any micropulse feature would appear within the first 25–35 lag values; the rest of this skewness curve probes the subpulse structure.

The average results for PSR 2016+28 (Fig. 5) show both strong similarities and differences with the PSR 0950+08 curves. The profile is more complex than for PSR 0950+08, broader and composed of two unequal components. The autocorrelation function shows the presence of the second subpulse at an 11 ms time lag and the micropulse breakpoint at ~ 250 μs. In the skewness curve, the tendency of the profile to fall off more steeply than it rises is confirmed quantitatively. There is some blending here of the notched structure between the two peaks into the leading and trailing edge features. This reduces the minimum value attained by the curve, since the notch and the outer edges of the profile have the opposite sense of skewness.

The average low resolution skewness curve has a number of properties. Most important is the double-troughed feature already mentioned in the single pulse section. The first feature is preceded by a zero-level section indicating oppositely skewed but similar shapes for the two subpulses. The individual skewnesses of the subpulse components have opposite senses and hence cancel each other initially. After time lags greater than ~ 3 ms, though, one of them starts to dominate. This is supported by the single-pulse analysis of PSR 0950+08 above, which also has a "cross-skewness" trough. The sense of skewness compatible with this curve is one in which the outside edge of either one of the subpulses has a longer time scale than the inside portion of that same subpulse. This interpretation also requires the skewness of the first subpulse in the window to be slightly more pronounced than the second.

At less than the 1% skewness level, there is no evidence for micropulse asymmetry in these data. Since the skewness analysis is statistical it can only be used to comment on the systematic properties of the micropulses. It is not clear whether this high degree of symmetry is maintained in individual micropulses; a full investigation of this would require a sixth-order moment analysis to estimate the "skewness variance."

IV. DISCUSSION

We have presented a general method for analyzing time series asymmetries and have applied it to pulsar signals. The skewness analysis sensitively probes asymmetries occurring on a variety of time scales. Furthermore, it is not dependent on an explicit identification of the feature being explored, removing a source of bias from the results. We have also shown both empirically and analytically that this technique is able to identify time series asymmetries in the presence of noise and when the individual features are closely spaced.

a) Observational Results

A number of interesting results have arisen from the skewness analysis of PSR 0950+08 and PSR 2016+28. The micropulse emission from both (quite different) pulsars seems to be highly symmetric *on average*. The average symmetry may reflect a precise symmetry of individual micropulses; however, we cannot rule out the possibility that micropulses are asymmetric with nearly

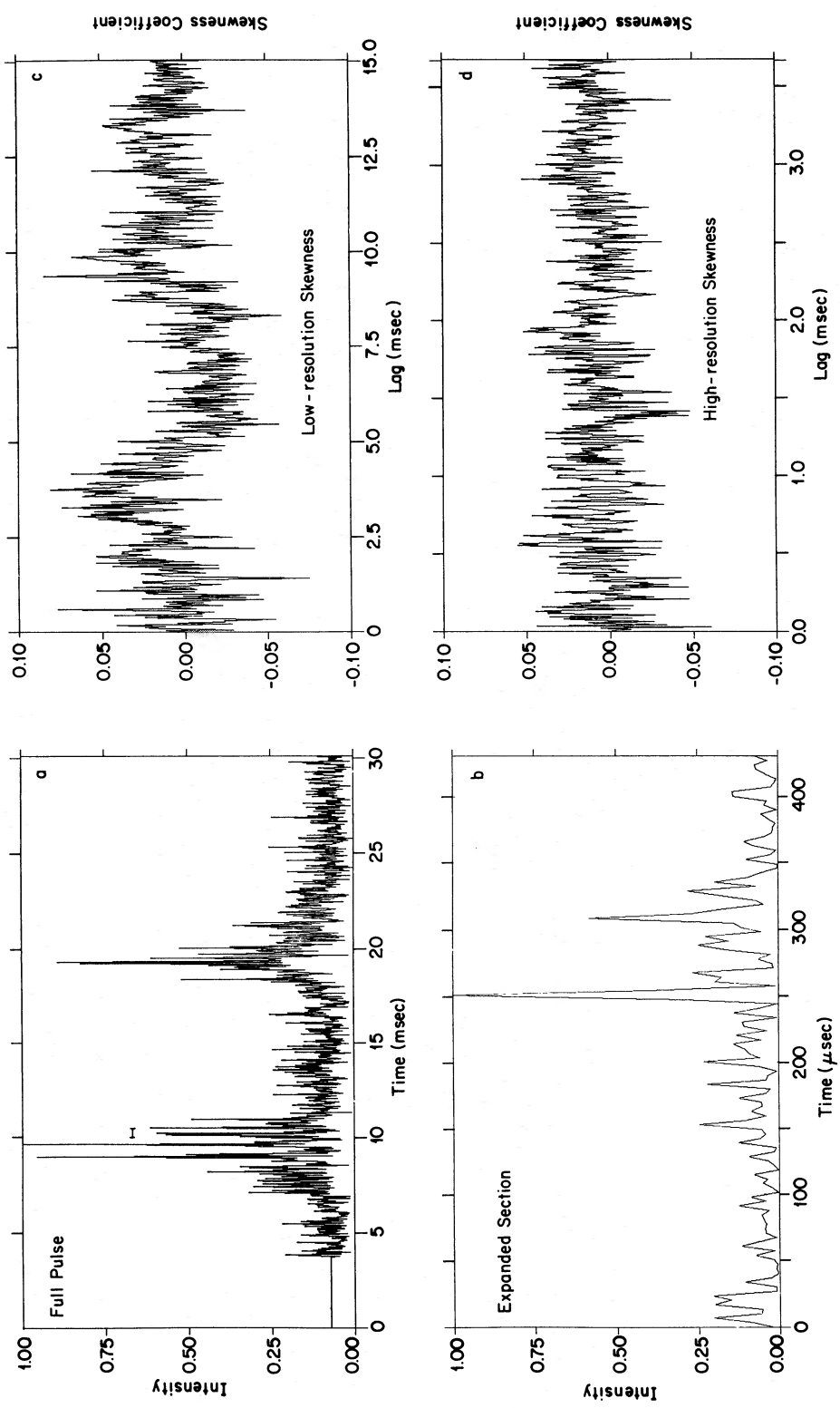

FIG. 4.—Skewness analysis of a single pulse from PSR 2016+28. Same quantities as in Fig. 2.

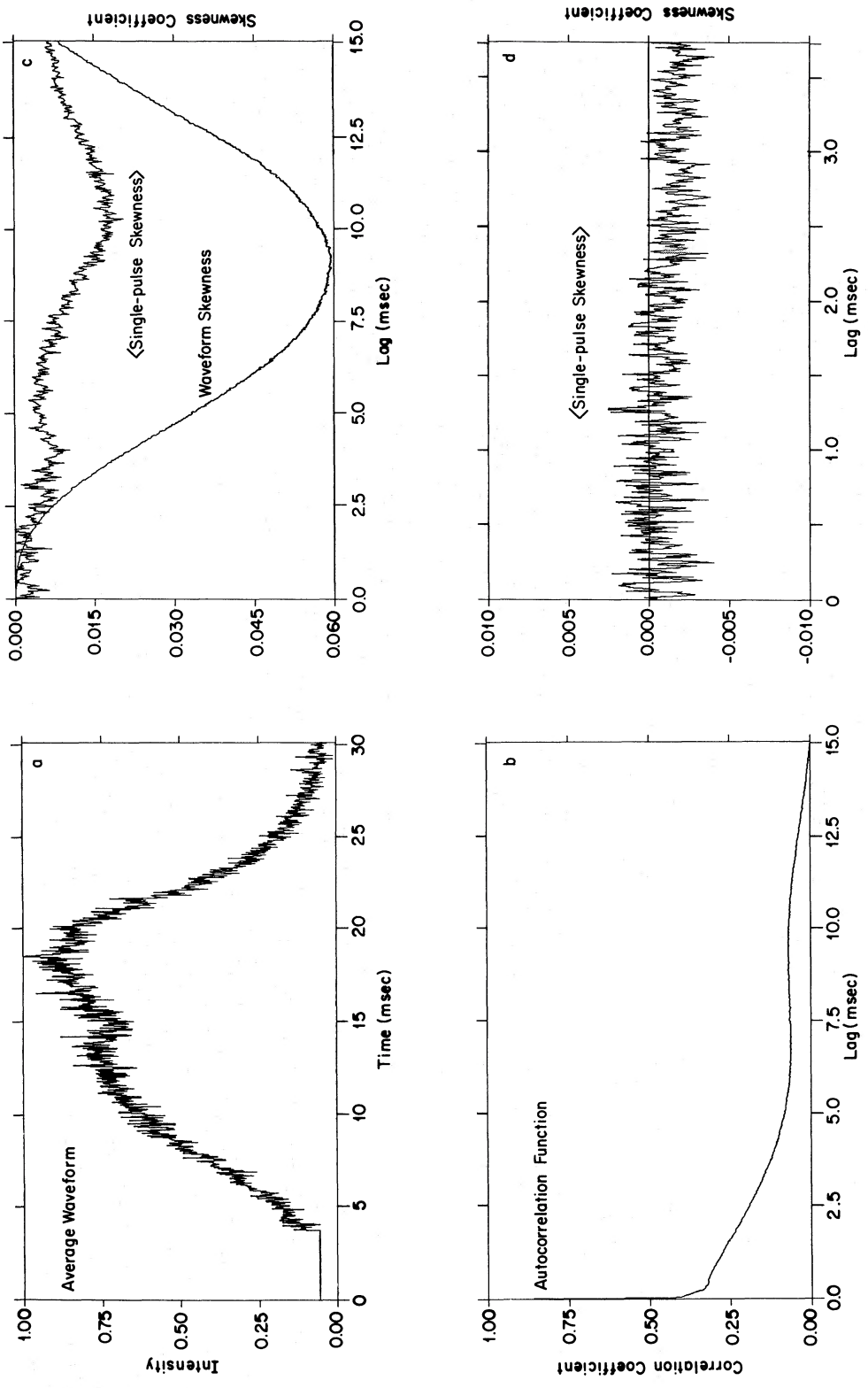

FIG. 5.—Average skewness analysis of 978 pulses from PSR 2016+28

equal probabilities for positive and negative skewness. At the very least, we can conclude that there is no *preferred* sense of micropulse skewness.

As for subpulse skewness, the sense of skewness is the same for both pulsars, although we do not suppose that this will hold for all pulsars. Of greatest significance is the fact that the average subpulse skewness follows that of the average waveform, at least in sense if not in detail. It is well known that the average waveform results from two effects: (1) a multiplicative one whereby features in single pulses have amplitudes determined in part by their position in the pulse window (strong subpulses tend to occur near local waveform maxima); (2) the frequency of occurrence of subpulses at given longitudes (strong but infrequent subpulses occur in low intensity regions of the waveform). The detection of significant subpulse skewness suggests that subpulse shapes are influenced by the multiplicative aspect of the waveform. The waveform is wider than subpulses due to subpulse jitter, and the waveform skewness is on a larger time scale than the subpulse skewness. The enhanced waveform skewness is clearly due to the arrival-time jitter of asymmetric subpulses, but it is also clear (Fig. 5 of Hankins and Cordes 1981) that the jitter itself for PSR 0950+08 is time asymmetric: strong subpulses sometimes occur with their peaks on the leading edge of the waveform but almost never occur on the trailing edge.

b) Physical Interpretation

Physically, we can interpret the skewness measurements in terms of polar cap models as they are understood at present (Cheng and Ruderman 1980; Arons 1979, 1981). Within such models we can furthermore make the distinction (as in the Introduction) between angular beaming and temporal modulations as possible causes for observed intensity variations. The correspondence of subpulse and average waveform asymmetries lends support to the view that subpulses represent angular beams of emission that are instantaneous versions of the time-average emission beam (i.e., the waveform). A similar conclusion has been reached (Rickett and Cordes 1981) on the basis of the polarization and frequency dependence of subpulse emission.

Rickett and Cordes have also shown that micropulses are inconsistent with an angular beaming interpretation, primarily because micropulse separations are evidently frequency independent (Boriakoff 1981), whereas subpulse widths and separations depend on frequency in a manner consistent with angular beaming effects in polar cap models. Assuming micropulses represent temporal modulations we must ask why, *on average*, their rise and decay times are identical. Such temporal modulations may arise from fluctuations in particle injection processes or from coherence fluctuations. Both processes could easily produce asymmetric emission features since the initiation of particle creation and acceleration of coherent radiation may depend on different physics than the termination of these processes. One possibility is that asymmetries are produced locally but with either sense of skewness so that, even over an individual micropulse, the asymmetry is washed out.

We wish to thank V. Boriakoff and T. Hankins for graciously allowing us to use their data and for providing helpful suggestions during the course of this work. R. Lovelace also made useful comments regarding the motivation and implementation of the skewness analysis. R. Isaacman aided the early development of this paper through numerous helpful and heated discussions. Finally, it is a pleasure to thank J. Weisberg for his encouragement during the preparation of this paper. The Arecibo Observatory is part of the National Astronomy and Ionosphere Center, which is operated by Cornell University under contract with the National Science Foundation.

APPENDIX

SKEWNESS MEASURES OF STOCHASTIC PROCESSES

a) Third-Order Moments

The second-order moment analysis of a time series has become a common tool in astronomy, although it is more often referred to as an autocorrelation or spectral analysis. Since we rely heavily in our time skewness analysis on third-order correlation functions, we discuss them here along with definitions of the statistical measures which accompany them. We also apply this skewness analysis to an extension of Rickett's (1975) amplitude-modulated noise model of pulsar emission.

Consider a real continuous random process, $I(t)$. The ensemble average of the autocorrelation function is defined as

$$\langle R_I(\tau)\rangle \equiv \left\langle \int_0^L I(t)I(t+\tau)\,dt \right\rangle, \tag{A1}$$

where the duration of the time series is L (which should be implicitly understood in the expressions that follow). The

autocorrelation function is real, symmetric about the origin, and contains information about the time scales of amplitude variations in the signal.

The third-order correlation of the same random process is

$$\langle C_I(\tau_1,\tau_2)\rangle \equiv \left\langle \int I(t)I(t+\tau_1)I(t+\tau_2)\,dt \right\rangle, \tag{A2}$$

whose two-dimensional Fourier transform, the bi-spectrum, is used extensively in oceanography and geophysics. We are interested in a restricted, one-dimensional version of this correlation,

$$\langle T_I(\tau)\rangle = \langle C_I(0,\tau)\rangle, \tag{A3}$$

or

$$\langle T_I^+(\tau)\rangle \equiv \langle C_I(0,\tau)\rangle = \left\langle \int I^2(t)I(t+\tau)\,dt \right\rangle, \tag{A4a}$$

and

$$\langle T_I^-(\tau)\rangle \equiv \langle C_I(\tau,\tau)\rangle = \left\langle \int I(t)I^2(t+\tau)\,dt \right\rangle, \tag{A4b}$$

for $\tau \geq 0$ only. The function $\langle T_I(\tau)\rangle$ is *not* in general symmetric about the origin. In fact, $\langle T_I(\tau)\rangle$ is only symmetric if $I(t)$ is composed only of time fluctuations which are symmetric about their centroids.

The skewness function in our analysis is just a measure of the asymmetry of $\langle T_I(\tau)\rangle$ (cf. Frenkiel and Klebanoff 1967),

$$K_I(\tau) \equiv T_I^+(\tau) - T_I^-(\tau). \tag{A5}$$

For a deterministic $I(t)$, like those functions shown in Figure 6, we gain no new insight from $K_I(t)$ and do just as well considering $I(t)$. However, for studying the structure of a random process (such as the micropulse features of a pulsar signal), we need a skewness measure that does not require us to explicitly locate each feature. This is the job performed by calculating $T_I(\tau)$ (and subsequently the skewness function $K_I[\tau]$), because it throws away information about the location of each feature and collapses the skewness information down to a region localized about the origin.

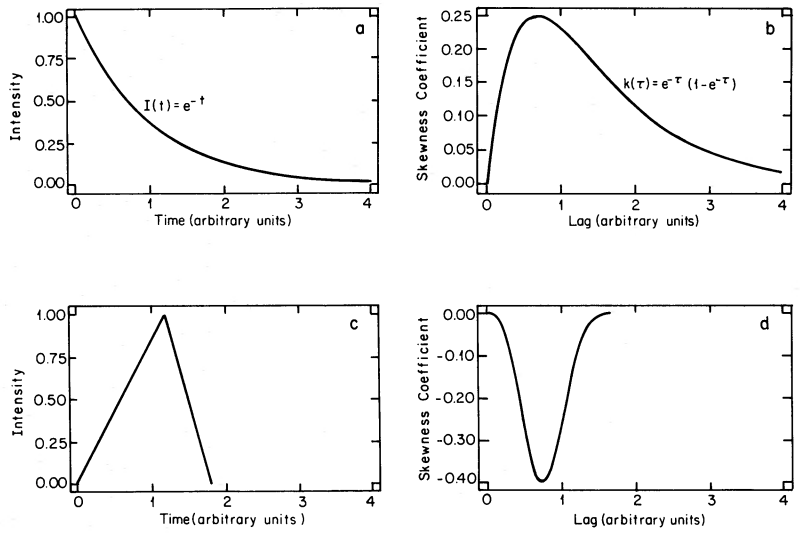

FIG. 6.—Skewness functions of deterministic signals: (*a*) one-sided exponential and (*b*) its positive-going skewness function; (*c*) a triangle function with a negative-going skewness function.

A number of characteristics of $K_I(\tau)$ are apparent in Figure 6. First of all, the sign of the function determines the sense of the temporal skewness: positive (negative) $K_I(\tau)$ values indicate structure which rises more rapidly (slowly) than it decays.

Second, note that by definition the skewness function will equal zero at the origin and that any excursion away from zero will occur on time scales equal to the temporal fluctuations being studied. This, of course, can lead to a blending of skewness features if there is modulation of $I(t)$ occurring on several time scales at once, a point we consider further below.

Third, the normalization of $K_I(\tau)$ is chosen by analogy with the autocorrelation function to be

$$k_I(\tau)=\frac{K_I(\tau)}{T_I(0)} \tag{A6}$$

so as to limit the range of the skewness function to the internal $[-1, +1]$. This last condition strictly holds only for positive definite time series, such as the intensity of a pulsar signal.

b) Application to an Empirical Model for Pulsar Signals

We now apply this skewness analysis to the amplitude-modulated noise (AMN) model of pulsar emission. In this empirical description, the predetection signal is represented as the product of a statistically stationary noise process and a nonstationary amplitude modulation,

$$y(t)=\alpha(t)n(t), \tag{A7}$$

where $\alpha(t)$ is real and $n(t)$ is zero-mean complex Gaussian noise. Assuming that the effects of dispersion smearing have been removed from the signal (see, e.g., Hankins and Rickett 1975) and that multipath scattering in the interstellar medium can be ignored, the fluctuation time scale of the signal is determined by the impulse response function of the receiver, $h(t)$. Rickett has shown that the average autocorrelation of such a signal is

$$\langle R_I(\tau)\rangle=\langle R_{\alpha^2}(\tau)\rangle|R_h(0)|^2+\langle R_{\alpha^2}(0)\rangle|R_h(\tau)|^2. \tag{A8}$$

The second term in this expression falls to zero at times greater than $\sim 1/\Delta\nu$ for critically sampled data ($\Delta\nu$ is the receiver bandwidth) so that the noise merely contributes a "zero-lag spike" to the autocorrelation function. Similarly, by expressing the sixth-order moment of complex Gaussian processes

$$\langle x_1x_2x_3x_4x_5x_6\rangle$$

as a sum of all the unique products of second-order moments we find the analogous result for the third moment,

$$\langle T_I(\tau)\rangle=2|R_h(0)|^3\langle T_{\alpha^2}(\tau)\rangle+4|R_h(0)||R_h(\tau)|^2\langle T_{\alpha^2}(0)\rangle. \tag{A9}$$

Note that the zero-lag spike in this case is $2/3\ \langle T_I(0)\rangle$ as compared with $1/2\ \langle R_I(0)\rangle$ for the autocorrelation function. Again, the only effect of the noise process on the average third moment occurs on time scales $\lesssim 1/\Delta\nu$.

Concentrating attention, then, on the detected value of the amplitude modulating function,

$$A(t)\equiv\alpha^2(t), \tag{A10}$$

we want to break it into the product of two functions,

$$A(t)=S(t)\mu(t), \tag{A11}$$

the first describing subpulse variations in the signal, the second the micropulse contribution. The micropulse function can be further specified by assuming a stationary shot-noise model

$$\mu(t)=\sum_i a_i g(t-t_i), \tag{A12}$$

where the "shape function", $g(t)$, is deterministic and the a_i's are drawn from an amplitude distribution with finite moments up to sixth order.

We now calculate the skewness function of $I(t)$ in terms of the skewness functions of $S(t)$ and $\mu(t)$. From equation (A9) it follows that

$$\langle T_I(\tau)\rangle \propto \langle T_A(\tau)\rangle \tag{A13}$$

for times greater than $1/\Delta\nu$, and, if we assume subpulse and micropulse variations are not correlated with each other, equation (A11) indicates that

$$\langle T_A(\tau)\rangle = \langle T_s(\tau)\rangle\langle T_\mu(\tau)\rangle. \tag{A14}$$

If the rate of occurrence (per unit time) of the micropulse is η, then

$$\langle \mu(t)\rangle = \eta\langle a\rangle \int g(t-t')\,dt', \tag{A15}$$

and

$$\langle \mu(t_1)\mu(t_2)\rangle' \equiv \langle \mu(t_1)\mu(t_2)\rangle - \langle \mu(t)\rangle^2 = \eta\langle a^2\rangle \int g(t_1-t')g(t_2-t')\,dt', \tag{A16}$$

since $\langle \mu(t_1)\rangle = \langle \mu(t_2)\rangle$. Then the third-order moment of $\mu(t)$ is

$$\begin{aligned}\langle \mu(t_1)\mu(t_2)\mu(t_3)\rangle = {} & \langle \mu(t_1)\rangle\langle \mu(t_2)\rangle\langle \mu(t_3)\rangle + \langle \mu(t_1)\rangle\langle \mu(t_2)\mu(t_3)\rangle' + \langle \mu(t_2)\rangle\langle \mu(t_1)\mu(t_3)\rangle' \\ & + \langle \mu(t_3)\rangle\langle \mu(t_1)\mu(t_2)\rangle' + \eta\langle a^3\rangle \int g(t_1-t')g(t_2-t')g(t_3-t')\,dt'.\end{aligned} \tag{A17}$$

From the definition of the skewness function, equation (A5), we then have

$$\langle K_\mu(\tau)\rangle = \langle \mu^2(t)\mu(t+\tau)\rangle - \langle \mu(t)\mu^2(t+\tau)\rangle, \tag{A18}$$

which, after using equation (A17), becomes

$$\langle K_\mu(\tau)\rangle = \eta\langle a^3\rangle K_g(\tau), \tag{A19}$$

with

$$K_g(\tau) \equiv \int g^2(t)g(t+\tau)\,dt - \int g(t)g^2(t+\tau)\,dt. \tag{A20}$$

Thus, the skewness function of the micropulse shot sequence is simply proportional to that of the micropulse shape, $g(t)$.

We now want to determine

$$K_A(\tau) = T_s^+(\tau)T_\mu^+(\tau) - T_s^-(\tau)T_\mu^-(\tau), \tag{A21}$$

where ensemble averaging brackets should be understood on all quantities that follow. Using equation (A17) and

$$R_\mu(\tau) = \eta\langle a^2\rangle \int g(t)g(t+\tau)\,dt, \tag{A22}$$

we have

$$T_\mu^\pm(\tau) = \langle \mu(t)\rangle^3 + \langle \mu(t)\rangle\left[2R_\mu(\tau) + R_\mu(0)\right] + \eta\langle a^3\rangle T_g^\pm(\tau), \tag{A23}$$

from which we find

$$K_A(\tau)=\eta\langle a^3\rangle\left[T_s^+(\tau)T_g^+(\tau)-T_s^-(\tau)T_g^-(\tau)\right]$$
$$+\langle\mu\rangle^3\left[1+R_\mu(0)/\langle\mu\rangle^2\right]K_s(\tau)+2\langle\mu\rangle R_\mu(\tau)K_s(\tau) \quad \text{(A24)}$$

If we further assume that on micropulse time-scales

$$T_s^+(\tau)\approx T_s^-(\tau)=T_s^\pm(0), \quad \text{(A25)}$$

and, without any loss of generality set $\langle\mu\rangle=1$ (thus attributing nonstationary intensity fluctuations to $S(t)$; see eq. [A11]), then

$$K_A(\tau)\approx\frac{\langle a^3\rangle}{\langle a\rangle^3}\frac{k_{g(\tau)}}{(\eta W_1)^2}T_s^\pm(0)+\left\{1+\frac{\langle a^2\rangle}{\langle a\rangle^2\eta W_2}\left[1+2r_\mu(\tau)\right]\right\}K_s(\tau), \quad \text{(A26)}$$

where

$$r_\mu(\tau)\equiv R_\mu(\tau)/R_\mu(0)\leq 1, \quad \text{(A27)}$$

and

$$W_1\equiv\left\{\frac{\left[\int g(x)\,dx\right]^3}{\int g^3(x)\,dx}\right\}^{1/2}, \qquad W_2\equiv\frac{\left[\int g(x)\,dx\right]^2}{\int g^2(x)\,dx}, \quad \text{(A28)}$$

are characteristic micropulse time scales with $W_1\approx W_2$. If we normalize the skewness function according to

$$k_A(\tau)=K_A(\tau)/T_A(0), \quad \text{(A29)}$$

and use

$$T_A(0)=T_s^\pm(0)T_\mu^\pm(0), \quad \text{(A30)}$$

with

$$T_\mu^\pm(0)=1+\frac{\langle a^3\rangle}{\langle a\rangle^3(\eta W_1)^2}+\frac{3\langle a^2\rangle}{\langle a\rangle^2\eta W_2}, \quad \text{(A31)}$$

we can simplify equation (A26):

$$k_A(\tau)=\frac{1}{\left(1+1/f_1^2+3/f_2\right)}\left[\left(\frac{1}{f_1^2}\right)k_g(\tau)+(1+1/f_2)k_s(\tau)+\frac{2}{f_2}k_s(\tau)r_\mu(\tau)\right], \quad \text{(A32)}$$

where

$$f_1\equiv\left(\frac{\langle a\rangle^3}{\langle a^3\rangle}\right)^{1/2}\eta W_2, \qquad f_2\equiv\eta W_1\frac{\langle a\rangle^2}{\langle a^2\rangle}, \quad \text{(A33)}$$

are two filling factors (e.g., if all amplitudes are the same, then $\eta W_{1,2}\ll 1$ implies that micropulses are few and far between, while $\eta W_{1,2}\gg 1$ implies extensive overlap).

Equation (A32), then, expresses the skewness function of $I(t)$ in terms of the subpulse and micropulse skewness functions. How do these three terms contribute to $k_A(\tau)$? For small values of the filling factors the expression becomes

$$k_A(\tau)\approx k_g(\tau)+\frac{f_1^2}{f_2}\left[1+r_\mu(\tau)\right]k_s(\tau). \quad \text{(A34)}$$

On micropulse time scales the second term above is insignificant compared to the first, and we have $k_A(\tau)\approx k_g(\tau)$. In other words, estimating the high resolution skewness function of the intensity is essentially the same as measuring it for the deterministic micropulse shape function. Additionally, on subpulse time scales, when $k_g(\tau)$ and $r_\mu(\tau)$ are essentially zero, we have $k_A(\tau)\approx(f_1^2/f_2)k_s(\tau)$. That is, the estimated skewness function is proportional to the subpulse skewness, the proportionality depending on how fully the area under the subpulse is "filled" with micropulses.

When the filling factor becomes very large we lose track of the micropulse skewness entirely and

$$k_A(\tau)\approx k_s(\tau), \tag{A35}$$

which is essentially zero on micropulse time scales. This is just an expression of the central limit theorem, the final distribution arising from the superposition of densely packed micropulses of any shape. At intermediate values of the f's (of order unity) equation (A32) gives in principle a correction for the estimation of $k_g(\tau)$ from $k_A(\tau)$:

$$k_g(\tau)\approx 2\{2k_A(\tau)-k_s(\tau)[1+r_\mu(\tau)]\}. \tag{A36}$$

c) Estimation Errors

Finally, we consider in a qualitative fashion the error arising from the estimation of $\langle k_A(\tau)\rangle$ by a finite averaging process

$$\langle k_A(\tau)\rangle_{\rm est}=\frac{1}{N}\sum_{i=1}^{N} k_{A_i}(\tau), \tag{A37}$$

where $k_{A_i}(\tau)$ is the skewness function associated with the ith realization of $A(t)$ (in our case the ith pulsar pulse). General considerations give an estimate of the third moment estimation error as

$$\Delta k_A(\tau)\equiv\frac{|\langle k_A(\tau)\rangle_{\rm est}-\langle k_A(\tau)\rangle|}{\langle k_A(\tau)\rangle}\approx\frac{\langle a^6\rangle^{1/2}}{\langle a^3\rangle}\frac{1}{\sqrt{N}}, \tag{A38}$$

where N is the number of micropulses in the ensemble average. Greatest estimation problems will arise, then, for amplitude distributions that are highly skewed and, of course, for pulsars with few micropulses.

Note that this same analysis holds for additive receiver noise preset in the system, although for this case we know the amplitude distribution

$$\left.\frac{\langle a^6\rangle^{1/2}}{\langle a^3\rangle}\right|_{\rm noise}=4.47,$$

and the value of N is equal to the number of independent time samples in the data set, typically a very large number. Hence, receiver noise is not a significant contribution to the skewness estimation error.

REFERENCES

Armstrong, J. W., and Rickett, B. J. 1981, *M.N.R.A.S.*, **194**, 623.
Arons, J. 1979, *Space Sci. Rev.*, **24**, 437.
_____. 1981, in *IAU Symposium 95, Pulsars*, ed. R. Wielebinski and W. Siebert (Dordrecht: Reidel), in press.
Benford, G. 1977, *M.N.R.A.S.*, **179**, 311.
Boriakoff, V. 1981, *Ap. J.*, submitted.
Cheng, A. F., and Ruderman, M. A. 1980, *Ap. J.*, **235**, 576.
Cordes, J. M. 1976, *Ap. J.*, **210**, 780.
Cordes, J. M., and Hankins, T. H. 1979, *Ap. J.*, **233**, 981.
Ferguson, D. C. 1979, *Bull. AAS*, **11**, 426.
Frenkiel, F. N., and Klebanoff, P. S. 1967, *Phys. Fluids*, **10**, 507.
Hankins, T. H., and Boriakoff, V. 1978, *Nature*, **276**, 45.
Hankins, T. H., and Cordes, J. M. 1981, *Ap. J.*, submitted.
Hankins, T. H., and Rickett, B. J. 1975, *Methods Comput. Phys.*, **14**, 55.
Kirk, J. G., and ter Haar, D. 1978, *Astr. Ap.*, **66**, 359.
Rickett, B. J. 1975, *Ap. J.*, **197**, 185.
_____. 1977, *Ann. Rev. Astr. Ap.*, **15**, 479.
Rickett, B. J., and Cordes, J. M. 1981, in *IAU Symposium 95, Pulsars*, ed. R. Wielebinski and W. Sieber (Dordrecht: Reidel), in press.
Ritchings, R. T. 1976, *M.N.R.A.S.*, **176**, 249.
Ruderman, M. A., and Sutherland, P. G. 1975, *Ap. J.*, **196**, 51.
Taylor, J. H., Manchester, R. N., and Huguenin, G. R. 1975, *Ap. J.*, **195**, 513.
Weisskopf, M. C., Sutherland, P. G., Katz, J. I., and Canizares, C. R. 1978, *Ap. J. (Letters)*, **223**, L17.

JAMES M. CORDES and DAN STINEBRING: Space Sciences Building, Cornell University, Ithaca, NY 14853